Received: 22 July 2020 | Revised: 2 September 2020 | Accepted: 23 September 2020

DOI: 10.1111/jace.17517

ORIGINAL ARTICLE

Journal of the American Ceramic Society

Mg-bearing quartz solid solutions as structural intermediates between low and high quartz

Alessio Zandona[1] | **Bernd Rüdinger**[2] | **Joachim Deubener**[1]

[1]Institute of Non-Metallic Materials, Clausthal University of Technology, Clausthal-Zellerfeld, Germany

[2]Central Research and Development, Schott AG, Mainz, Germany

Correspondence
Alessio Zandona, Institute of Non-Metallic Materials, Clausthal University of Technology, Clausthal-Zellerfeld, Germany.
Email: alessio.zandona@tu-clausthal.de, ale.zando92@gmail.com

Abstract

Glass powder samples of cordierite composition (doped with 8 mol% TiO_2) were heat-treated to produce a series of increasingly SiO_2-enriched Mg-bearing quartz solid solutions (Qss). The obtained materials were then analyzed by X-ray diffraction: Rietveld structural refinements revealed that Mg-bearing Qss phases possess trigonal symmetry and a compositionally dependent intermediate structural arrangement between those of low and high quartz. High-temperature diffraction measurements were performed up to 700°C to characterize the thermal expansion behavior of the crystals. At SiO_2-rich compositions, a reversible high-to-intermediate inversion of the quartz structure is observed, which shifts with increasing stuffing to lower temperatures than the conventional 573°C for pure quartz. Similarities and differences to the better-established Li-bearing Qss are discussed in the text.

KEYWORDS

glass-ceramics, magnesium aluminosilicate, quartz inversion, quartz solid solutions, X-ray diffraction

1 | INTRODUCTION

Structural analogies between the crystalline polymorphs of SiO_2 and other natural or synthetic compounds of different composition were already identified in the early days of X-ray crystallography, such as cristobalite-like carnegieite[1] and tridymite-like nepheline[2] (both with stoichiometry $NaAlSiO_4$). These structures have been specifically termed *stuffed derivatives* if the partial substitution of Si^{4+} by Al^{3+} (or by other lower valence cations) in the tetrahedral sites leads to the incorporation of additional extra-framework cations[3] to maintain overall charge neutrality.[4]

Prime examples of the above-described category of compounds are the quartz-like solid solutions obtainable in the magnesium aluminosilicate (MAS),[5,6] lithium aluminosilicate (LAS),[6,7] and zinc aluminosilicate (ZAS)[6] compositional systems, as well as in their mutual mixtures.[6-10] These quartz solid solutions (Qss) are of particular interest in materials science for representing the major component of LAS glass-ceramics with near-zero thermal expansion and high thermal shock resistance.[11] Moreover they act as crystalline precursors during the crystallization of cordierite from glass[5,12,13]; the production of high-strength materials based on the formation of Si-rich Qss in MAS glasses has also been suggested.[14,15]

Li-bearing Qss are by far the most investigated members of this family: it is known that they display a high-quartz-like structure (hereafter HQss) at room temperature, from the composition of the endmember β-eucryptite ($LiAlSiO_4$)[16] down to approximately 82.5 mol% SiO_2 content.[17-20] At a lower extent of structural stuffing, however, the room-temperature framework collapses into that of low quartz (hereafter LQss), as often indirectly identified through the positive thermal expansion of the phases.[6] These structural changes

are relatively abrupt and they are mirrored by the linear compositional dependence of the quartz inversion temperature (T_c in the following), from the conventional value of 573°C in pure quartz[21] down to cryogenic temperatures.[19,20]

The structural relations of Qss in the MAS system appear less clear. The seminal work of Schreyer and Schairer[5] identified their occurrence and reported, in the vicinity of the SiO_2 endmember, about a downshift of the low-high quartz inversion from the conventional value of 573°C.[21] This latter observation has been then confirmed through dilatometric studies.[14,15] The average structure was initially refined in terms of a high-quartz-like lattice, with Mg accommodated in octahedral cavities within the *c*-channels of the framework.[22]. The position of the Mg atoms showed a temperature dependence and was made responsible for the appearance of broad superstructure reflections.[23] However, more recent investigations[24,25] assigned a trigonal symmetry to these phases (ie LQss) even at a Mg- and Al-rich stoichiometry ($Mg_{0.5}AlSiO_4$) and from room temperature up to 1273 K. This inference would better agree with the positive thermal expansion displayed by Mg-bearing Qss, in contrast to the negative one shown by Li-bearing HQss.[6,26]

Consequently, a comprehensive investigation of Qss in the MAS compositional system was formulated within this study and performed mainly by X-ray diffraction (XRD). The results shed new light on the compositional variation of the average structure and thermal behavior of these phases, which are of crucial importance for their technological applications in glass-ceramics.

TABLE 1 Lattice parameters *a* and *c*, unit cell volumes (UCV) at room temperature as well as critical inversion temperatures T_c obtained for all investigated samples from (HT-)XRD. Numbers in parentheses provide the uncertainty of the last digits

Sample	*a* (Å)	*c* (Å)	UCV (Å^3)	T_c (°C)
1155	4.999 (2)	5.421 (4)	117.33 (9)	492 (10)
1135	5.012 (2)	5.416 (3)	117.82 (8)	394 (10)
1000_100	5.034 (2)	5.410 (2)	118.74 (5)	323 (10)
1000_66	5.051 (2)	5.405 (2)	119.42 (7)	282 (15)
1000_44	5.060 (2)	5.405 (3)	119.83 (7)	195 (20)
1000_33	5.082 (2)	5.393 (3)	120.61 (7)	—
1000_28	5.080 (2)	5.395 (1)	120.59 (5)	—
1000_24	5.095 (2)	5.385 (3)	121.07 (7)	—
1000_16	5.107 (2)	5.380 (2)	121.53 (7)	—
1000_8	5.124 (2)	5.374 (2)	122.19 (6)	—
1000_4	5.141 (1)	5.368 (2)	122.85 (6)	—
950_100	5.119 (2)	5.370 (3)	121.88 (7)	—
950_75	5.125 (2)	5.367 (2)	122.10 (7)	—
950_50	5.135 (2)	5.365 (2)	122.52 (6)	—
950_20	5.149 (1)	5.360 (2)	123.06 (5)	—
950_10	5.154 (1)	5.358 (2)	123.28 (5)	—
950_4	5.168 (1)	5.355 (1)	123.85 (4)	—

2 | EXPERIMENTAL PROCEDURES

2.1 | Sample preparation

The melting procedure of the parent glass has been described elsewhere.[13] The chosen stoichiometry was that of the mineral cordierite ($2MgO{\cdot}2Al_2O_3{\cdot}5SiO_2$), doped with 8 mol% TiO_2 as a crystallization additive, since previous investigations revealed that this addition catalyzed the formation of Qss and accelerated the evolution of its lattice parameters towards those of low quartz during further annealing.[13] The glass was grinded into a powder (5 μm < D_{50} < 6.5 μm and D_{90} < 35 μm, as from a Cilas 1064 laser particle size analyzer) and ceramized according to the following time-temperature program: a 5 K min^{-1} ramp to 950°C or 1000°C, an isothermal hold for up to 100 hours, passive furnace cooling. The nomenclature of the samples was defined according to the scheme: *temperature in degrees centigrade_time in hours*. After its full characterization, specimen 1000_100 was subjected to a further controlled annealing (in the XRD heating chamber) at 1135°C for 30 minutes. The obtained powder, named 1135, was analyzed and then again heat-treated at 1155°C for 60 minutes, obtaining sample 1155. The ensemble of all prepared samples is listed in Table 1.

2.2 | X-ray diffraction

Room-temperature characterization of the crystallized powders was performed on an X´Pert Pro MPD diffractometer (Malvern Panalytical), operated at 40 mA/45 kV and equipped with a copper X-ray tube, rotating powder sample holder and a Pixcel1D detector (255 channels, 14 mm active length). The incident beam optics included: 0.5° divergence slit, 10 mm mask, 0.04 mm Soller slits and 1° antiscatter slit. The diffracted beam optics included: 0.04 mm Soller slits and a Ni filter. Measurements were performed in the range 5-140° 2θ with a step size of 0.013° 2θ and time-per-step of 51 seconds (total measurement duration of 35 minutes).

The high-temperature measurements took place on a similar Empyrean diffractometer (Malvern Panalytical), operated at 40 mA/40 kV (copper X-ray tube and Pixcel1D detector) and equipped with a high-temperature chamber (HTK 1200N, Anton Paar), whose temperature calibration has been previously described.[27] The incident beam optics included: a 0.125° divergence slit, a 4 mm mask, a BBHD mirror, 0.04 mm Soller slits and a 0.5° antiscatter slit. The diffracted beam optics included: a 7.5 mm antiscatter slit and 0.04 mm

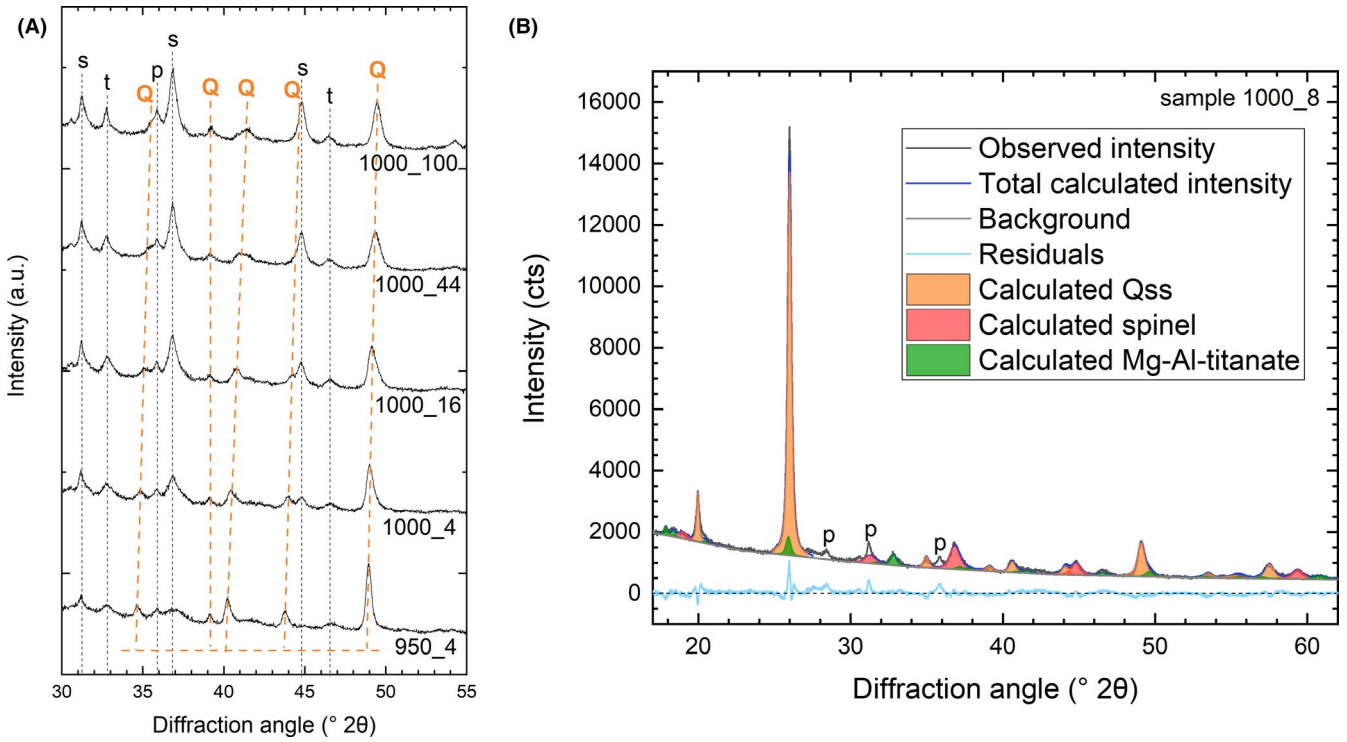

FIGURE 1 A, Selected range of the diffractograms collected at room temperature from some of the samples (*s* for spinel, *t* for pseudobrookite-like Mg-Al-titanate, *p* for protoenstatite and *Q* for Qss); B, results of the Rietveld refinement performed for sample 1000_8 (*p* labels the weak protoenstatite peaks neglected during this analysis) [Color figure can be viewed at wileyonlinelibrary.com]

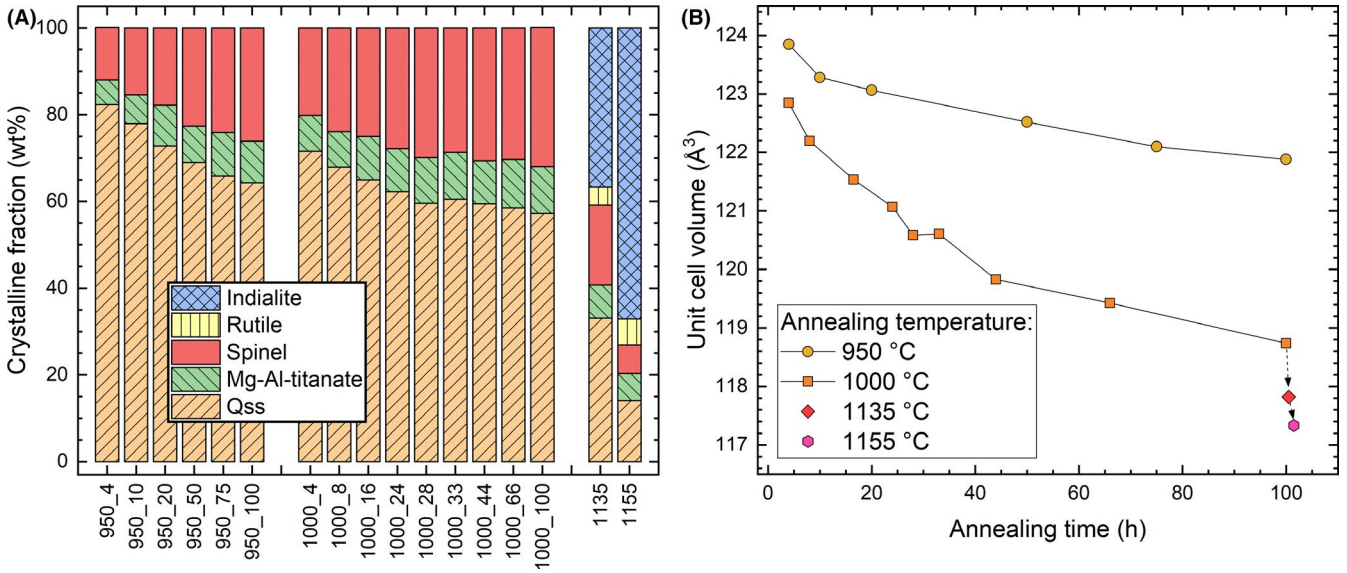

FIGURE 2 A, Evolution of the crystalline assemblage of the analyzed powders according to the applied time-temperature program (the amorphous fraction is neglected); B, variation of the unit cell volume of Qss in the samples during isothermal holds at 950°C, 1000°C and the further annealing of 1000_100 at 1135°C and 1155°C [Color figure can be viewed at wileyonlinelibrary.com]

Soller slits. The samples were measured at room temperature and every 20°C between 60°C and 700°C, with the following measurement parameters: range 5-100° 2θ, step size 0.026 ° 2θ, time-per-step 40 seconds (total measurement duration of 10 minutes).

Rietveld analysis was executed on the software HighScore Plus (Malvern Panalytical), employing structural models for Qss (based on the trigonal structure ($P3_221$) of Mg-bearing LQss[24]), Mg-Al-titanate [COD 2002319], spinel [COD 9001364], rutile [COD 9015662] and indialite [COD

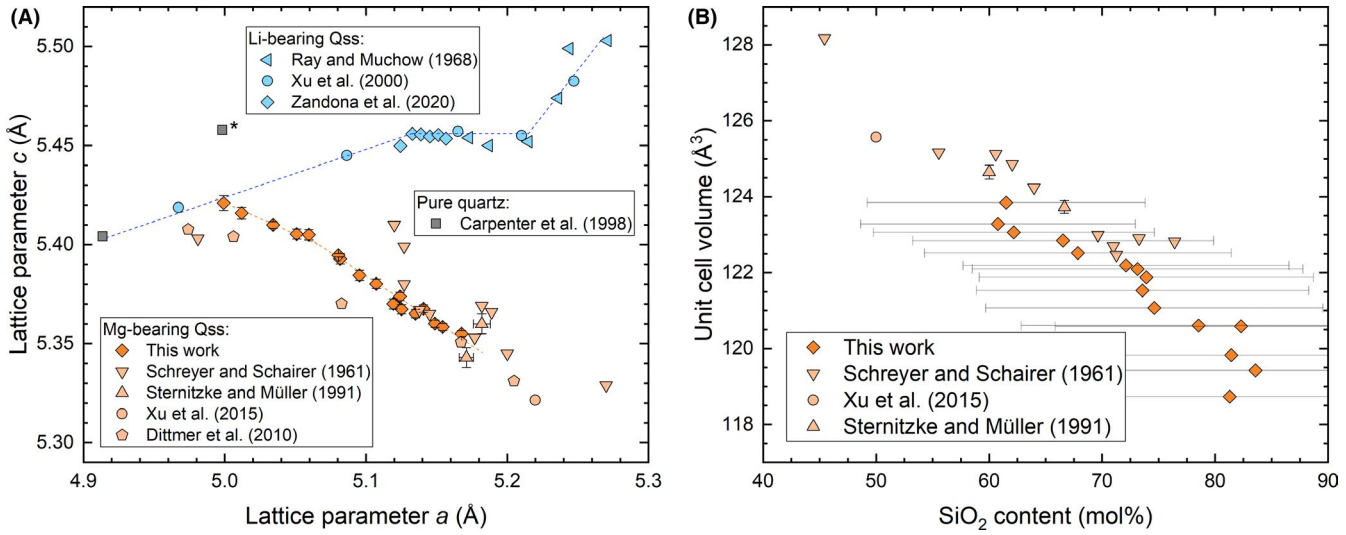

FIGURE 3 A, Plot of the room-temperature lattice parameters obtained for Mg-bearing Qss within this work and from some literature references,[5,14,24,26] as well as for pure quartz[31] (* labels the value pertaining to high quartz at 600°C). The plot contains also the values obtained from literature sources for Li-bearing Qss,[10,18,20] for the purposes of comparison. Lines are only meant as a guide to the eye. B, Compositional dependence of the unit cell volume (UCV) of Qss, including the data from this work (SiO_2 content computed from the Mg *sof* in Table 2) and from some literature references (nominal compositions of the parent glasses) [Color figure can be viewed at wileyonlinelibrary.com]

TABLE 2 Atomic coordinates and Mg site occupation factor (*sof*) fitted during Rietveld refinements of the XRD measurements performed at room temperature on all samples. The last column reports the inferred average SiO_2 content of the crystals from the values of the Mg *sof*. Numbers in parentheses provide the uncertainty of the last digits

Sample	Si/Al, x	O, x	O, y	O, z	Mg, x	Mg, *sof*	SiO_2 (mol%)
1000_100	0.476 (1)	0.6008 (9)	0.754 (1)	0.804 (1)	0.177 (8)	0.09 (2)	81 (16)
1000_66	0.480 (1)	0.5969 (8)	0.756 (1)	0.811 (1)	0.151 (9)	0.08 (2)	84 (17)
1000_44	0.481 (1)	0.5951 (8)	0.762 (1)	0.815 (2)	0.143 (8)	0.09 (2)	81 (16)
1000_33	0.484 (1)	0.5919 (8)	0.764 (2)	0.808 (1)	0.114 (7)	0.11 (2)	79 (16)
1000_28	0.483 (1)	0.5987 (8)	0.763 (1)	0.816 (2)	0.100 (9)	0.09 (2)	82 (16)
1000_24	0.487 (1)	0.5934 (8)	0.765 (1)	0.812 (2)	0.097 (6)	0.13 (3)	75 (15)
1000_16	0.485 (1)	0.5938 (7)	0.766 (1)	0.815 (2)	0.089 (6)	0.13 (3)	74 (15)
1000_8	0.488 (1)	0.5924 (7)	0.766 (1)	0.814 (2)	0.073 (6)	0.14 (3)	72 (14)
1000_4	0.490 (1)	0.5925 (7)	0.767 (1)	0.816 (2)	0.061 (5)	0.17 (3)	67 (13)
950_100	0.486 (2)	0.5923 (8)	0.767 (2)	0.814 (2)	0.054 (8)	0.13 (3)	74 (15)
950_75	0.483 (1)	0.5937 (7)	0.767 (2)	0.818 (2)	0.069 (6)	0.13 (3)	73 (15)
950_50	0.488 (1)	0.5926 (7)	0.767 (1)	0.814 (2)	0.049 (6)	0.16 (3)	68 (14)
950_20	0.487 (1)	0.5938 (6)	0.772 (1)	0.813 (1)	0.073 (4)	0.19 (4)	62 (12)
950_10	0.489 (1)	0.5934 (6)	0.772 (1)	0.814 (1)	0.057 (4)	0.20 (4)	61 (12)
950_4	0.492 (1)	0.5922 (6)	0.772 (1)	0.810 (1)	0.049 (4)	0.19 (4)	62 (12)

1529492][28]; the peaks assignable to protoenstatite were conversely too weak to be reliably fitted. The background was approximated by linear interpolation through setpoints. After this, scale factors, lattice parameters, specimen shift, Caglioti profile and shape parameters were manually and successively added to the refinement, ascertaining convergence of the calculation after each step. The structure of Qss was then refined, enabling the *sof* of Mg and all symmetrically unconstrained atomic coordinates; refinement of the atomic displacement parameters proved instead unstable and was therefore omitted, fixing their values to those previously determined by other authors.[24] The uncertainty of the values was obtained multiplying by 3 the estimated standard deviations provided by the program. The obtained structures were sketched using

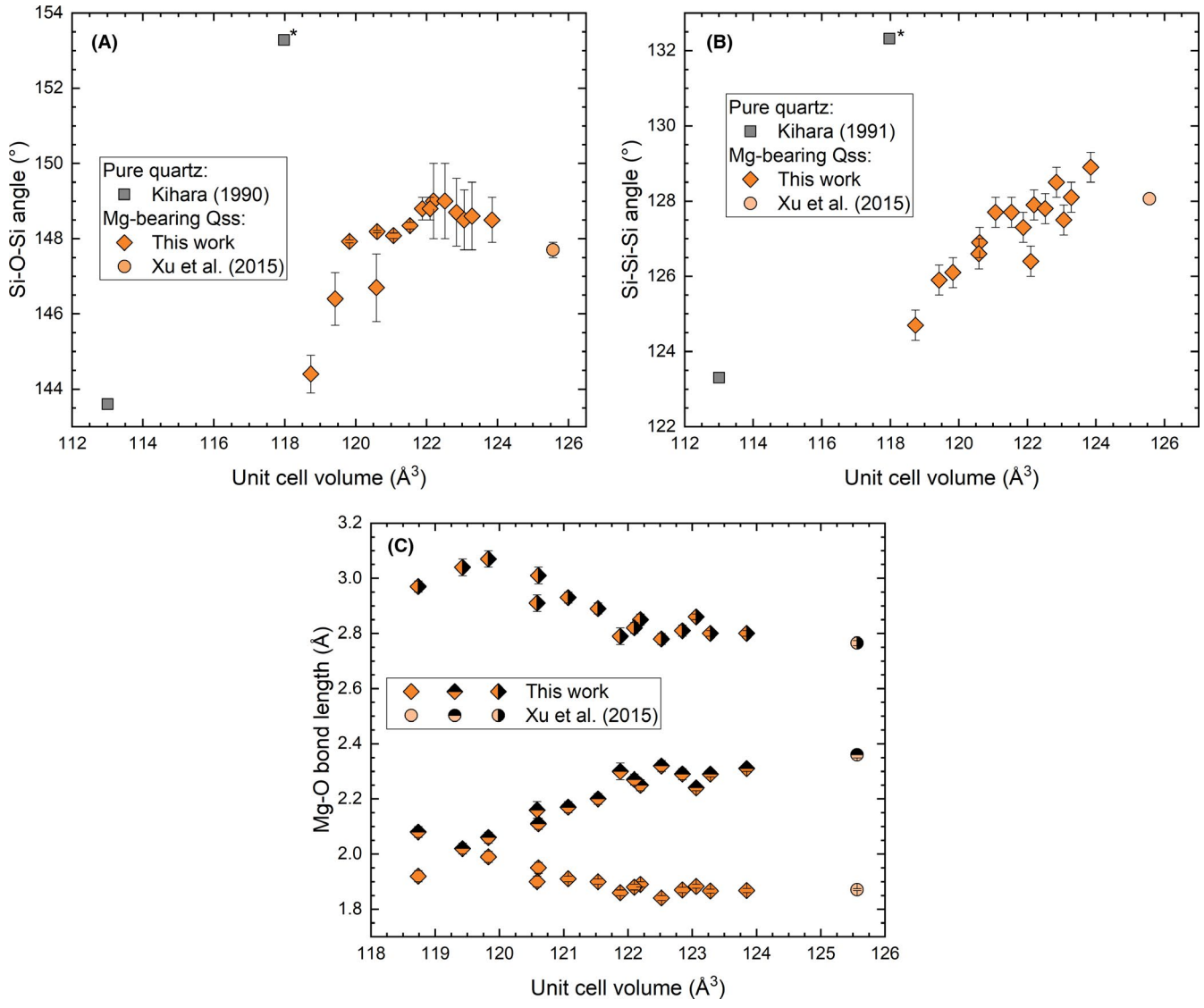

FIGURE 4 Correlation of the unit cell volumes of Qss and: A, the Si-O-Si angle, B, the Si-Si-Si angle in the tetrahedral helical chains defining the *c* channels and C, the Mg-O bond lengths in the Qss structure, as obtained from Rietveld refinements. The values of literature references[24,32] are reported for the purposes of comparison. (* labels the values pertaining to high quartz at 600°C) [Color figure can be viewed at wileyonlinelibrary.com]

the software VESTA.[29] No structural refinement of Qss was applied in samples 1135 and 1155, due to their more complex phase assemblage.

3 | RESULTS

All the samples that were ceramized at 950°C and 1000°C contained a similar crystalline assemblage after the annealing procedure, namely Qss, spinel, pseudobrookite-like Mg-Al-titanate and a very weak additional signature assignable to protoenstatite (Figure 1). The samples obtained after treatment at 1135°C and 1155°C also contained rutile and indialite, in agreement with previous investigations of glass-ceramics of the same composition.[13,30] Increasing annealing temperatures and time induced a growth in the amount of spinel that was accompanied by a shift of the Qss diffraction peaks to higher angles (Figure 2). The observed shift mirrored an overall shrinkage of the unit cell (Figure 2B), consistent with a gradual Si-enrichment of this phase and similarly inferred by other authors.[13,14]

The mutual variation of the *a* and *c* lattice parameters obtained in the samples at room temperature is compiled in Table 1 and evaluated in Figure 3: the data exhibit a coherent trend, in good agreement with the values from Xu et al (2015)[24] and within the scatter range of other available references for Mg-bearing Qss.[5,14,26] An increase in *a* is interestingly accompanied by a decrease in *c* in the MAS system, whereas a contemporary overall growth of both parameters is known from the LAS system and here reported for comparison.[7,18,20] In addition, the MAS data does not seem to directly converge toward the values of pure low or high quartz.[31] The

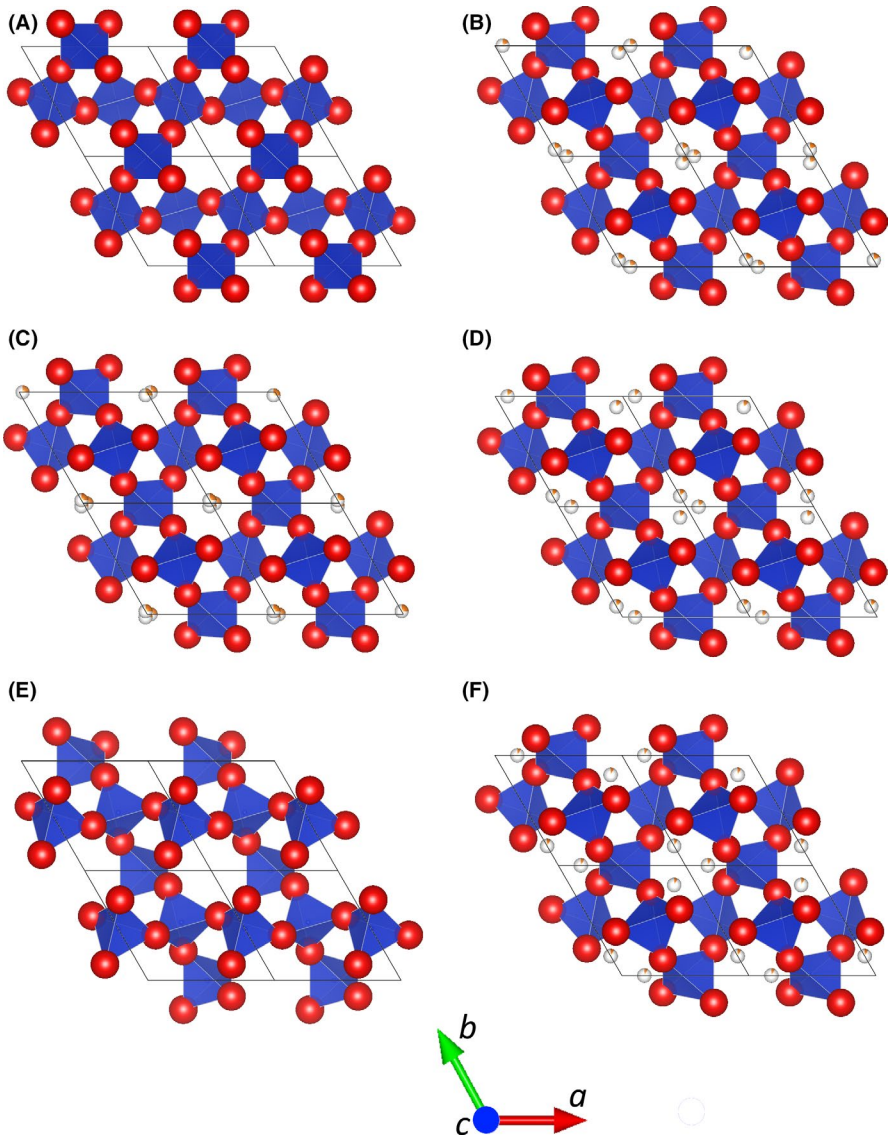

FIGURE 5 Schematic representation of the structures of: A, high quartz,[32] B, Mg-bearing Qss in sample 1000_4, C, Mg-bearing Qss from 24, D, Mg-bearing Qss in sample 1000_24, E, low quartz[32] (mind the author´s different origin choice) and F, Mg-bearing Qss in sample 1000_100, all viewed along the *c* direction (red spheres are O atoms, blue tetrahedra stand for the mixed Si/Al site and partially filled orange spheres represent the Mg atoms with corresponding site occupation factor) [Color figure can be viewed at wileyonlinelibrary.com]

LQss-to-HQss transition of the LAS samples is particularly manifested by an evident and abrupt change in the slope of the data points; in the data produced within this work, a change in slope is barely visible at an *a* value of approximately 5.08 Å.

An overall dependence of the structural parameters of Qss on the composition of the crystals is expected from literature.[5] Within this work, the Qss stoichiometry had to be estimated through the *sof* of Mg obtained during Rietveld refinements, since all specimens were obtained from the same parent glass. The computed values (Figure 3B and Table 2) matched satisfactorily the scattered trend of the available literature sources,[5,24,26] which were indicated based on the nominal composition of the parent glass annealed to form Qss. However, the determination using the *sof* proved less successful at comparatively high SiO_2 content (see the four rightmost data points in Figure 3B). Since the determination of *sof*'s during Rietveld refinements is far less reliable than that of unit cell volumes, the latter values were employed as a "compositional proxy" to plot the variation of some key structural features of Qss in Figure 4. The corresponding values obtained from literature for pure low and high quartz[32] and a Qss of composition $Mg_{0.5}AlSiO_4$[24] are also reported.

As in the latter reference, the trigonal character of the Mg-bearing Qss structure emerges also from the results of this work (Figure 5). Moreover a gradual transition is discernible from a low-quartz-like configuration towards high-quartz-like features, although the process appears to saturate at an intermediate state. Si-O-Si angles are strongly affected at low unit cell volumes (ie high SiO_2 content) (Figure 4A) and soon stabilize around ~148°, in accordance with the recent results of Xu et al.[24] The longer-range Si-Si-Si angles within the Qss helical chains parallel to *c* show a continuous variation over the studied compositional range (Figure 4B), manifesting a gradual tetrahedral tilt that leads to an increasing "pseudo-hexagonality" of the *c*-channels (see the progression in Figure 5F,D,B,C). Such relations are in agreement with the description provided by Xu et al,[24,25] who referred to a tetrahedral rotation angle δ and remarked the intermediate value obtained for Mg-Qss at 299 K (~9.4°), between

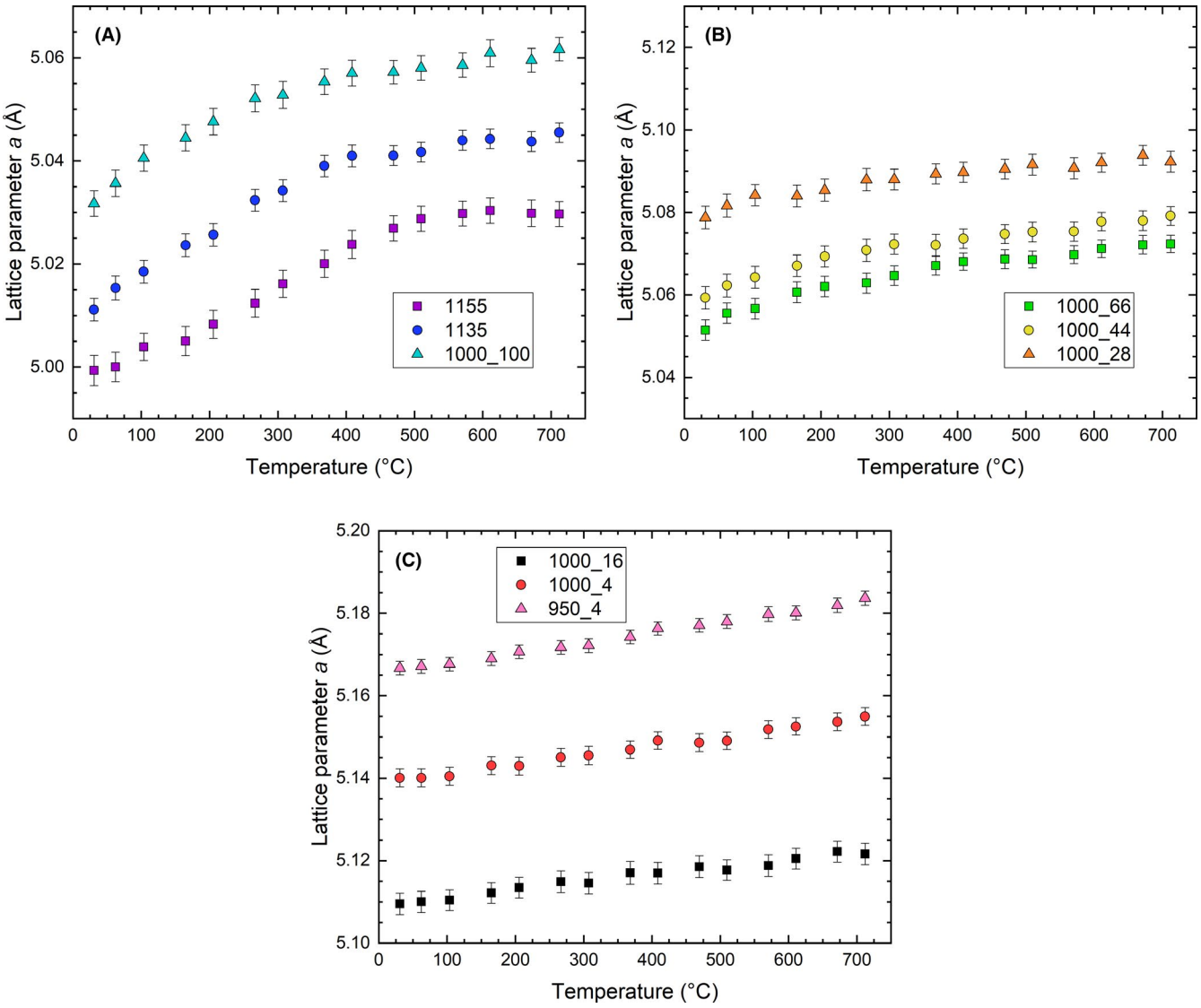

FIGURE 6 Variation of the *a* lattice parameter of Qss as a function of temperature obtained from HT-XRD measurements of: A, samples 1155, 1135 and 1000_100, B, samples 1000_66, 1000_44 and 1000_28, C, samples 1000_16, 1000_4, 950_4 [Color figure can be viewed at wileyonlinelibrary.com]

those of room-temperature low quartz (15.8°) and high quartz (0°). In turn, the distorted octahedral oxygen coordination of Mg appears to achieve progressively higher regularity with increasing unit cell volume (ie decreasing SiO_2 content, Figure 4C). The remarkable *x*-displacement of the Mg positions from the center of the *c*-channels at high SiO_2 (well visible in Figure 5F) may indeed only represent an artefact of the Rietveld refinements, possibly coupled with the above-mentioned unreliable determination of the Mg *sof*.

Subsequently, HT-XRD measurements were applied to some representative samples to investigate the LQss-HQss transition previously described by other authors.[5,14,15] Figures 6 and 7 report the obtained *a* and *c* lattice parameters from room temperature to 700°C: all samples display positive thermal expansion, which appears invariably almost linear along the *c*-direction, possibly due to the comparatively higher uncertainty associated with these values. In turn, the *a* parameters clearly display two expansion regimes in the SiO_2-richer specimens, manifesting a structural transition. This transition shifted towards lower temperatures and became less abrupt with decreasing SiO_2 content, until it was invisible in samples 1000_16, 1000_4 and 950_4 (as also reported by Xu et al[25]). The critical inversion temperatures T_c (Table 1) were extracted from the curves pertaining to samples 1155, 1135, 1000_100, 1000_66, and 1000_44 using the double-tangent method; in the case of specimen 1000_28, T_c resulted instead too close to room temperature to enable a reliable determination.

4 | DISCUSSION

The obtained results demonstrate that stuffing of the structure of quartz in the MAS system leads to remarkably different effects than in the LAS one. Although an increase in the

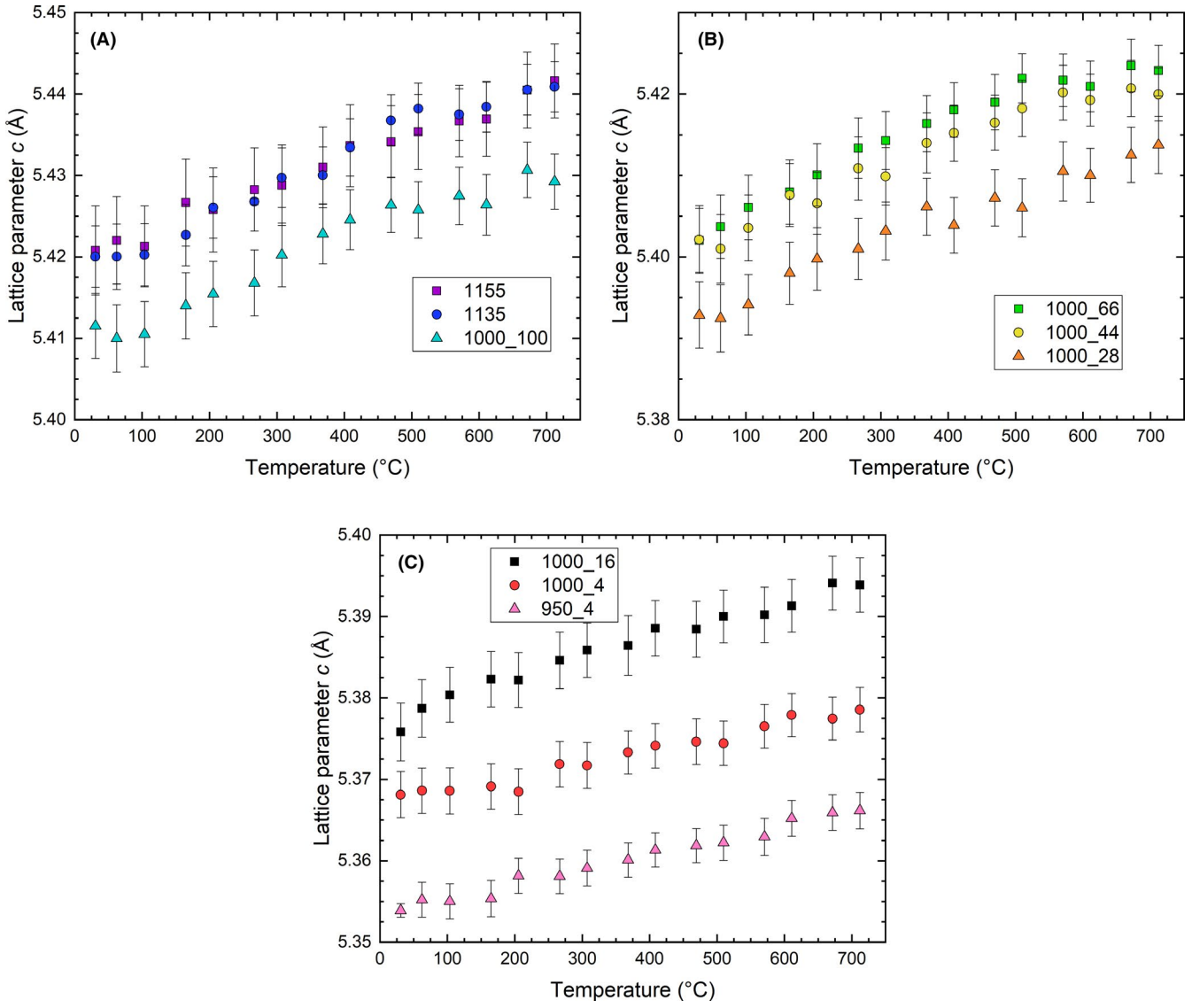

FIGURE 7 Variation of the *c* lattice parameter of Qss as a function of temperature obtained from HT-XRD measurements of: A, samples 1155, 1135 and 1000_100, B, samples 1000_66, 1000_44 and 1000_28, C, samples 1000_16, 1000_4, 950_4 [Color figure can be viewed at wileyonlinelibrary.com]

amount of dopants produces in both cases an expansion of the unit cell, the mutual variations of *a* and *c* show strikingly different behaviors. From a structural point of view, Li-bearing Qss are typically characterized in terms of either fully low-quartz- or high-quartz-like structures, respectively, at high and low SiO_2 content,[18,20] whereas recent results by other authors have already pointed out that this views are not applicable to Mg-bearing Qss.[24] In fact, according to the results of the present work, the average structure of these phases clearly resembles low quartz only at very low Mg + Al content and approaches a "pseudo-hexagonal" character with increasing doping, though never actually accomplishing the fully hexagonal symmetry typical of high quartz (at least at room temperature).

The occurrence of a compositionally triggered structural transition at room temperature in the samples analyzed within this work is deducible from the change in slope in the *a*-against-*c* plot (Figure 3 and more in detail Figure 8A), as this change is absent in the corresponding values at 600°C. The high-temperature points moreover agree well with the high quartz reference,[31] suggesting a certain continuity in their structural evolution, if not a fully high-quartz-like lattice at this temperature. Concerning the room-temperature data, they fail to align with either the high or the room-temperature low quartz references, again supporting the idea of an intermediate structural configuration.

Similar conclusions can be drawn from a correlation between unit cell volumes and critical inversion temperatures T_c. While T_c represents a single value only dependent on composition, unit cell volumes are also temperature-dependent through the thermal expansion of the crystals, closely connected to the low- or high-quartz-like character of their underlying structure. Consequently, only data points corresponding to crystals possessing the same basic framework (ie

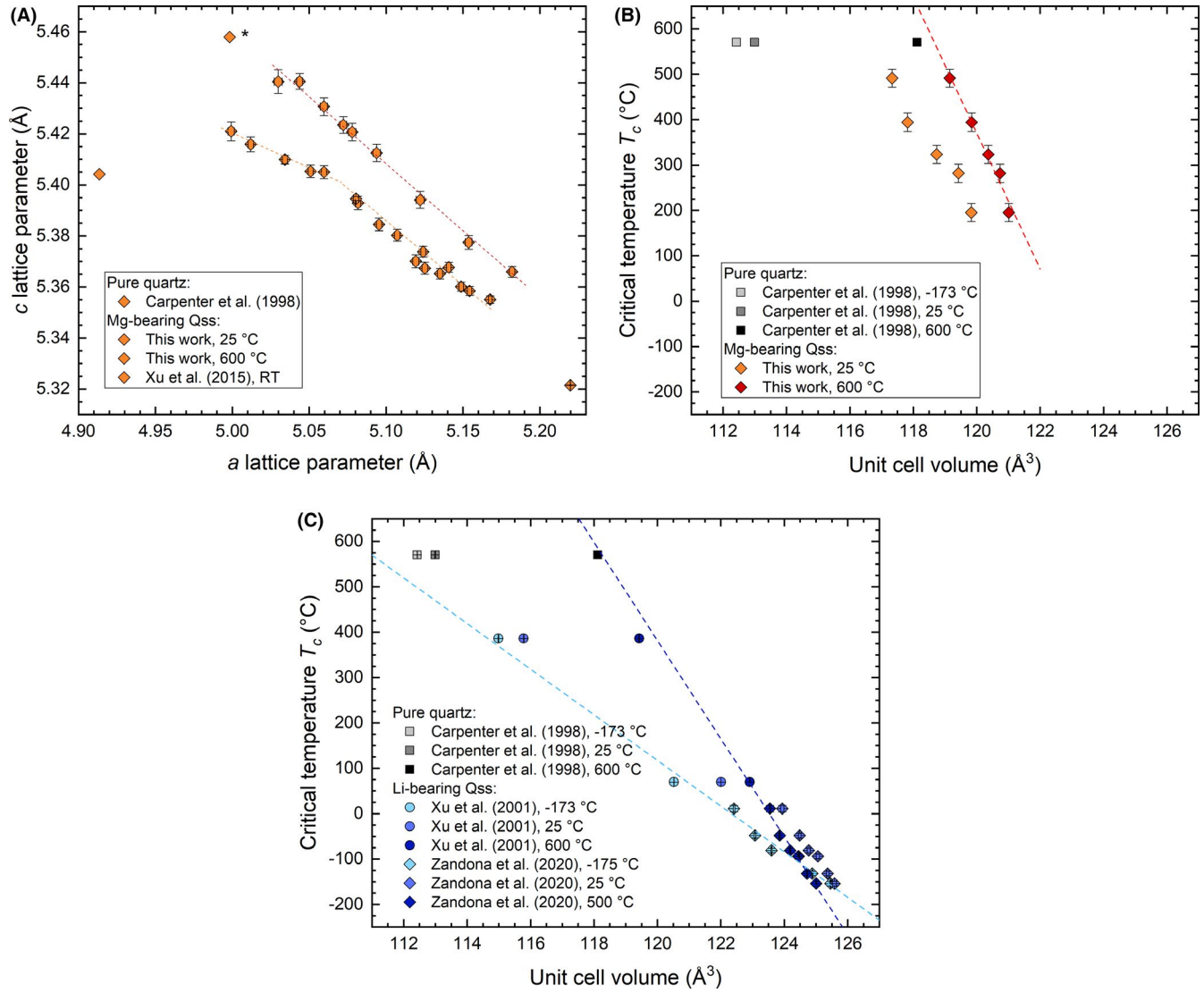

FIGURE 8 A, Plot of the lattice parameters obtained for Mg-bearing Qss within this work at room temperature and 600°C, as well as from literature references 24,31 (* labels the values pertaining to pure high quartz at 600°C, lines are only meant as a guide to the eye); B, Critical inversion temperature obtained for Mg-bearing Qss within this work, plotted against the respective unit cell volume at 25°C and 600°C, with the values obtained from literature for pure quartz[31]; C, a similar diagram for Li-bearing Qss, with values determined at −175°C, 25°C and 500/600°C degrees[19,20] [Color figure can be viewed at wileyonlinelibrary.com]

low or high quartz) and collected at the same temperature can possibly be in mutual accordance. This is in fact the case in the LAS system (Figure 8c): isothermal and isostructural straight lines could be drawn for T_c values plotted against unit cell volumes collected at −173°C (only LQss) and 500°C and above (only HQss). Room-temperature data are instead affected by the compositionally controlled LQss-HQss transition and do not plot on a simple straight line. Concerning Mg-bearing Qss (Figure 8B), the data points at 600°C agree reasonably with pure high quartz, while they plot between low and high quartz at room temperature. This observation further supports the assertion that Qss, at least at room temperature, cannot be treated as a directly isostructural phase with either low or high quartz, but rather as a *derivative* structure of low quartz (see also the discussion of the tetrahedral rotation angle δ in Xu et al[25]). The identified structural dissimilarities may then account for the positive thermal expansion of these crystals, in fact substantially lower than that of low quartz but much higher than that of high quartz,[31] as previously pointed out by other authors.[25,26]

5 | CONCLUSION

Careful examination of the average structure of Mg-bearing Qss crystallized in TiO_2-doped MAS glass-ceramics confirmed the trigonal character of these crystals[24] at room temperature and revealed intermediate structural features between those of pure low and high quartz. These observations were expanded by HT-XRD measurements, providing

a clear characterization of the thermal expansion of the crystals up to 700°C. Critical quartz inversion temperatures T_c were systematically determined in several samples at SiO_2-rich compositions and included in the crystallographic discussion. At temperatures above T_c, a high-quartz-like lattice is inferable.

ORCID

Alessio Zandona https://orcid.org/0000-0003-0091-9546

REFERENCES

1. Barth FW, Posnjak E. Silicate structures of the cristobalite type: I. The crystal structure of α-carnegieite (NaAlSiO4). Zeitschrift für Kristallographie - Crystalline Materials. 1932;81(1):135–41.
2. Schiebold E. Zur Struktur von Nephelin und Analcim. Science of Nature. 1930;18(31):705–6.
3. Buerger MJ. The stuffed derivatives of the silica structures. Am Miner. 1954;39(7–8):600–14.
4. Pauling L. The modern theory of valency. J Chem Soc. 1948;1461–7.
5. Schreyer W, Schairer J. Metastable solid solutions with quartz-type structures on the join SiO_2–$MgAl_2O_4$. Zeitschrift für Kristallographie. 1961;116(1–2):60–82.
6. Petzoldt J. Metastabile Mischkristalle mit Quarzstruktur mit Oxidsystem Li_2O-MgO-ZnO-Al_2O_3-SiO_2. Glastechn Ber. 1967;40:385–96.
7. Ray S, Muchow GM. High-quartz solid solution phases from thermally crystallized glasses of compositions (Li_2O, MgO)·Al_2O_3·nSiO_2. J Am Ceram Soc. 1968;51(12):678–82.
8. Beall GH, Karstetter BR, Rittler HL. Crystallization and chemical strengthening of stuffed beta-quartz glass-ceramics. J American Ceramic Society. 1967;50(4):181–90.
9. Zandona A, Rüdinger B, Hochrein O, Deubener J. Crystallization sequence within the keatite solid solution – cordierite mixed compositional triangle with TiO_2 as nucleating agent. J Non-Cryst Solids. 2019;505:320–32.
10. Ray S. Study of ordering in high-quartz solid solutions by substitutions affecting superlattice reflections. J Am Ceram Soc. 1973;56(1):42–5.
11. Bach H. Low Thermal Expansion Glass Ceramics. Springer-Verlag; 1995.
12. Müller R, Hübert T, Kirsch M. Untersuchungen zur Rekristallisation von Glaspulvern der Zusammensetzung 2 MgO · 2 Al_2O_3 · 5 SiO_2 · x TiO_2 (x≤0,7). Silikattechnik. 1986;37(4):111–4.
13. Zandona A, Rüdinger B, Hochrein O, Deubener J. Crystallization and SiAl ordering in cordierite glass-ceramics. J Non-Cryst Solids. 2018;498:160–6.
14. Dittmer M, Müller M, Rüssel C. Self-organized nanocrystallinity in MgO–Al_2O_3–SiO_2 glasses with ZrO_2 as nucleating agent. Mater Chem Phys. 2010;124:1083–8.
15. Hunger A, Carl G, Gebhardt A, Rüssel C. Ultra-high thermal expansion glass–ceramics in the system MgO/Al_2O_3/TiO_2/ZrO_2/SiO_2 by volume crystallization of cristobalite. J Non-Cryst Solids. 2008;354(52–54):5402–7.
16. Winkler HGF. Synthese und Kristallstruktur des Eukryptits, $LiAlSiO_4$. Acta Cryst. 1948;1(1):27–34.
17. Li C. The crystal structure of $LiAlSi_2O_6$ III (high-quartz solid solution). Zeitschrift für Kristallographie - Crystalline Materials. 1968;127(5–6):327–48.
18. Xu H, Heaney PJ, Beall GH. Phase transitions induced by solid solution in stuffed derivatives of quartz: a powder synchrotron XRD study of the $LiAlSiO_4$-SiO_2 join. Am Miner. 2000;85(7–8):971–9.
19. Xu H, Heaney PJ, Navrotsky A. Thermal expansion and structural transformations of stuffed derivatives of quartz along the $LiAlSiO_4$–SiO_2 join: a variable-temperature powder synchrotron XRD study. Phys Chem Miner. 2001;28(5):302–12.
20. Zandona A, Helsch G, Deubener J. Inversion of quartz solid solutions at cryogenic temperatures. J Am Ceram Soc. 2020;103:6630–8.
21. Heaney PJ, Veblen DR. Observations of the α-β phase transition in quartz: a review of imaging and diffraction studies and some new results. Am Miner. 1994;76:1018–32.
22. Schulz H, Hoffmann W, Muchow GM. The average structure of $Mg[Al_2Si_3O10]$, a stuffed derivative of the high-quartz structure*. Zeitschrift für Kristallographie - Crystalline Materials. 1971;134:1–27.
23. Schulz H. Influence of heat-treatment on the average structure of $Mg[Al_2Si_3O10]$, a stuffed derivative of the high-quartz structure. Zeitschrift für Kristallographie - Crystalline Materials. 1971;134:253–61.
24. Xu H, Heaney PJ, Yu P, Xu H. Synthesis and structure of a stuffed derivative of α-quartz, $Mg_{0.5}$ $AlSiO_4$. Am Miner. 2015;100(10):2191–8.
25. Xu H, Lü X, Heaney PJ, Ren Y. Structural behavior of a stuffed derivative of α-quartz, $Mg_{0.5}AlSiO_4$, at high temperature: an in situ synchrotron XRD study. Phys Chem Minerals. 2019;46(7):717–25.
26. Sternitzke M, Müller G. Crystal structure and thermal expansion of quartz-type aluminosilicates. J Mater Sci. 1991;26(11):3051–6.
27. Helsch G, Deubener J, Rampf M, Dittmer M, Ritzberger C. Crystallization and quartz inversion temperature of sol-gel derived LAS solid solutions. J Non-Cryst Solids. 2018;492:130–9.
28. Gražulis S, Chateigner D, Downs RT, Yokochi AFT, Quirós M, Lutterotti L, et al. Crystallography Open Database – an open-access collection of crystal structures. J Appl Crystallogr. 2009;42(4):726–9.
29. Momma K, Izumi F. VESTA3 for three-dimensional visualization of crystal, volumetric and morphology data. J Appl Crystallogr. 2011;44(6):1272–6.
30. Zandona A, Rüdinger B, Hochrein O, Deubener J. Chemical gradients at the surface of TiO_2-doped cordierite glass-ceramics. J Non-Cryst Solids. 2020;547:120298.
31. Carpenter MA, Salje EKH, Graeme-Barber A, Wruck B, Dove MT, Knight KS. Calibration of excess thermodynamic properties and elastic constant variations associated with the α ↔ β phase transition in quartz. Am Miner. 1998;83:2–22.
32. Kihara K. An X-ray study of the temperature dependence of the quartz structure. Eur J Mineral. 1990;2(1):63–78.

How to cite this article: Zandona A, Rüdinger B, Deubener J. Mg-bearing quartz solid solutions as structural intermediates between low and high quartz. *J Am Ceram Soc*. 2021;104:1146–1155. https://doi.org/10.1111/jace.17517